Characterization of an orange acceptor fluorescent protein for sensitized spectral fluorescence resonance energy transfer microscopy using a white-light laser

Yuansheng Sun
University of Virginia
Department of Biology
W. M. Keck Center for Cellular Imaging
McCormick Road
Charlottesville, Virginia 22904

Cynthia F. Booker
Sangeeta Kumari
University of Virginia Health System
Department of Medicine
and
Department of Cell Biology
Charlottesville, Virginia 22908

Richard N. Day
Indiana University
School of Medicine
Department of Cellular and Integrative Physiology
635 Barnhill Drive
Indianapolis, Indiana 46202

Mike Davidson
The Florida State University
National High Magnetic Field Laboratory
1800 East Paul Dirac Drive
Tallahassee, Florida 32310

Ammasi Periasamy
University of Virginia
Department of Biology
W. M. Keck Center for Cellular Imaging
and
Department of Biomedical Engineering
McCormick Road
Charlottesville, Virginia 22904

Abstract. Orange fluorescent proteins (FPs) are attractive candidates as Förster resonance energy transfer (FRET) partners, bridging the gap between green and red/far-red FPs, but they pose significant challenges using common fixed laser wavelengths. We investigated monomeric Kusabira orange 2 (mKO2) FP as a FRET acceptor for monomeric teal FP (mTFP) as donor on a FRET standard construct using a fixed-distance amino acid linker, expressed in live cells. We quantified the apparent FRET efficiency ($E\%$) of this construct, using sensitized spectral FRET microscopy on the Leica TCS SP5 X imaging system equipped with a white-light laser that allows choosing any excitation wavelength from 470 to 670 nm in 1-nm increments. The $E\%$ obtained in sensitized spectral FRET microscopy was then confirmed with fluorescence lifetime measurements. Our results demonstrate that mKO2 and mTFP are good FRET partners given proper imaging setups. mTFP was optimally excited by the Argon 458 laser line, and the 540-nm wavelength excitation for mKO2 was chosen from the white-light laser. The white-light laser generally extends the usage of orange and red/far-red FPs in sensitized FRET microscopy assays by tailoring excitation and emission precisely to the needs of the FRET pair. [DOI: 10.1117/1.3227036]

Keywords: Förster resonance energy transfer (FRET); spectral FRET (sFRET); fluorescence lifetime imaging FRET (FLIM-FRET); white-light laser; monomeric Kusabira orange 2 (mKO2); monomeric teal fluorescent protein (mTFP); instrument response function (IRF); protein–protein interactions.

Paper 09013RR received Jan. 15, 2009; revised manuscript received Jul. 13, 2009; accepted for publication Jul. 16, 2009; published online Sep. 16, 2009.

1 Introduction

The development of the green fluorescent protein (GFP)[1] and its mutant variants[2,3] in combination with fluorescence microscopy has led to a revolution in live-cell imaging techniques that allow visualization of dynamic protein interactions under physiological conditions. Förster resonance energy transfer (FRET) is an ideal technique to determine molecular distances or to show whether molecular complexes are present; this technique is increasingly taking center stage in the biomedical sciences.[4,5] FRET results in increased emission intensities from the acceptor (sensitized emission), while reducing the emission from the donor (quenching) and shortening the donor lifetime. Measurement of each event can provide direct proof of the transfer of energy, which in turn demonstrates the spatial relationship of the fluorophores. The efficiency of energy transfer is defined as the fraction of D excitation energy that is transferred to A, and is dependent on the inverse of the sixth power of the distance between D and A.[6,7]

Sensitized FRET microscopy is the most commonly used intensity-based method to monitor protein–protein interactions. This approach requires the identification and removal of

Address all correspondence to: Ammasi Periasamy, PhD, Director, W. M. Keck Center for Cellular Imaging (KCCI), Biology, Gilmer Hall (064), University of Virginia, McCormick Road, Charlottesville, VA 22904. Tel: 434-243-7602; Fax: 434-982-5210; E-mail: ap3t@virginia.edu

1083-3668/2009/14(5)/054009/11/$25.00

the spectral bleedthrough (SBT) components from FRET signals. These SBT contaminations result from the donor emission that is detected in the FRET channel, known as the donor SBT (DSBT), and the acceptor SBT (ASBT), which is caused by the direct excitation of the acceptor at the donor excitation wavelength. Both SBT contributions must be removed for accurate FRET measurements. Here, we use single-label reference specimens excited by donor and acceptor wavelengths and algorithm-based software to achieve a corrected signal.[8–10]

The accurate measurement of FRET signals requires fluorophores that are optimized for efficient energy transfer. Ideal donor and acceptor pairs will have high intrinsic brightness and will be photostable, while sharing a significant spectral overlap ($>30\%$) between the donor emission and acceptor absorption spectra. Among many FRET pairs cited in the literature, the combination of the *Aequorea*-based cyan FP (CFP) and yellow FP (YFP) has been most widely used.[11–15] Modifications to these FPs were made to improve their utility generally and particularly for FRET-based assays. For example, Venus is a brighter YFP with more efficient maturation and reduced pH and halide sensitivity.[16] Cerulean was developed from CFP and has a higher quantum yield and greater photostability.[17] Recently, Campbell introduced another FP, emitting in the cyan color spectrum, monomeric teal fluorescent protein (mTFP),[18] which was generated by the directed evolution of an optimized synthetic gene library based on the sequence of a tetrameric cyan protein, cFP484, from the coral *Clavularia*. Our earlier study showed that mTFP has many advantages, such as a higher quantum yield and improved brightness and photostability compared with Cerulean as a FRET donor for Venus.[19]

In addition, there are now many FPs with spectra spanning the orange to far-red that have optimized characteristics.[20–23] The orange FPs are very attractive candidates bridging the gap between green and the far-red FPs. The utility of an orange FP called monomeric Kusabira orange (mKO) as acceptor in FRET studies was discussed earlier.[24] The mKO is derived from CoralHue Kusabira-Orange (KO), which was cloned from the stony coral, whose Japanese name is Kusabira-ishi. Wild-type CoralHue KO forms a brightly fluorescent dimer and has been carefully engineered to form mKO that maintains the brilliance and pH stability of the parent protein. Recently, a fast-folding mutant of mKO named monomeric Kusabira orange 2 (mKO2) was introduced.[25]

In this study, we tested mKO2 as a FRET acceptor fluorophore for mTFP (donor) using sensitized spectral FRET (sFRET) microscopy and verified the measurements using fluorescence lifetime imaging (FLIM) microscopy in live cells. The sFRET imaging revealed that the diode-pumped solid-state (DPSS) 561 nm was not suitable for the acceptor (mKO2) excitation because this laser line is very close to the peak emission of mKO2 (565 nm), and thus limits the emission range of the FRET channel. We used a white-light laser (WLL; or supercontinuum laser) installed on the Leica TCS SP5 X imaging system. This laser emits a continuous spectrum from 470 to 670 nm, within which any individual excitation wavelength in 1-nm increments can be selected through acousto-optical tunable filter (AOTF). Given the flexibility of tunable wavelengths to choose a precise, tailored excitation for mKO2, this FP becomes a very useful FRET acceptor for mTFP.

2 Materials and Methods

2.1 *Expression Plasmids and Cell Transfection*

2.1.1 *mTFP and mKO2 plasmid*

The plasmid encoding the mTFP (gene bank accession: DQ676819) is available from Allele Biotechnology and Pharmaceuticals (San Diego, California). The mKO2 construct is available from MBL International (Woburn, Massachusetts). The plasmid encoding the FRET standard fusion protein consisting of Cerulean tethered to Venus by a 5 amino acid (aa) linker (SGLRS) was a gift from Steven Vogel (NIH).[26] The cDNA for Venus was obtained from Atsushi Miyawaki (RIKEN, Japan).[16] Vogel's plasmid was first used to generate the mTFP fusion protein (mTFP-5aa-Venus) by substituting the coding sequence for Cerulean with the cDNA for mTFP that was generated by polymerase chain reaction (PCR) with primers incorporating suitable restriction enzyme sites. The same parent plasmid was then used to generate the sequences that encode mTFP and the 5 aa linker coupled in-reading frame to the sequence encoding mKO2, creating the mTFP-5aa-mKO2 construct.

2.1.2 *Transfection of mouse pituitary cells*

Mouse pituitary GHFT1 cells[27] were maintained as monolayer cultures in Dulbecco's modified eagles medium (DMEM) containing 10% newborn calf serum. The cells were then transfected with the proceeding plasmid DNA by electroporation as described earlier.[28,29] The amount of DNA was kept constant for each transfection using empty vector DNA. Suspensions of the transfected cells were added drop-wise onto a sterile 25 mm^2 cover glass in culture dishes, and the cells were allowed to attach to the glass prior to gently flooding the culture dish with media. The cultures were maintained in an incubator for 24 h before imaging. The cover glass with attached cells was then inserted into a chamber filled with CO_2-independent medium and placed on the microscope stage.

2.2 *Instrumentation, Image Acquisition, and Analysis*

2.2.1 *Instrumentation for spectral FRET (sFRET) microscopy imaging*

A Leica TCS SP5 X system equipped with a $63\times/1.40$ NA oil-immersion objective lens was used for the sFRET imaging in this study. The TCS SP5 X scan head is mounted on a side port of a Leica DMI6000 motorized inverted microscope. The system consists of an 8-channel acousto-optical tunable filter (AOTF) for fast simultaneous control of eight laser lines and acousto-optical beamsplitter (AOBS) instead of dichroic mirror. The system works by a switching and tunable deflection mechanism. This allows various emission wavelengths to be efficiently routed to the three filter-free spectral photomultiplier tube (PMT) detectors that are continuously adjustable to a minimum bandwidth of 5 nm. Besides a conventional point scanner, which can be adjusted from 2 to 1400 Hz, the system also provides a fast resonant point scanner running constantly at 8000 Hz, allowing imaging speeds of 25 frames/second for 512×512 pixels and up to

250 frames/second for 512×16 pixels. The resonant scanner allows the rapid acquisition of spectral images, reducing the potential for photobleaching, and was thus used in our sFRET imaging. The system carries several laser modules. In our study, we used a 25-mW argon laser and a white-light laser (WLL). The WLL in the Leica TCS SP5 X imaging system consists of three fiber-based parts: a seed laser generating a pulsed emission at 80 MHz in the infrared, a strong pump source, and the supercontinuum fiber that emits a continuous spectrum from 470 to 670 nm.[30] An individual excitation wavelength in 1-nm resolution is selected through the AOTF. The critical advantage of this laser is that the investigators no longer need to select fluorophores based on the fixed laser lines carried by a microscope imaging system. Instead, the fluorophores can be chosen that are optimal for their experimental approaches, and the system can then be tuned specifically for the experiments. The imaging system is controlled by the Leica LAS AF software (http://www.leica-microsystems.com).

2.2.2 *Image acquisition and analysis in sFRET microscopy*

Earlier, we described the method for sFRET microscopy imaging.[10] Coverslips with cells expressing the mTFP-5aa-mKO2 construct or cells that expressed either mTFP alone or mKO2 alone were used. The cells expressing each fluorophore alone were used as reference controls to identify the SBT contamination in the FRET channel. Here, the 458-nm argon laser line was used to optimally excite the donor (mTFP), and the wavelength of 540 nm was chosen from the WLL for the acceptor (mKO2) excitation. In the SP5 X system, the power of an excitation laser is controlled through an AOTF, and the emission is spread spectrally by a prism and then guided to a spectrometer slit that allows any emission band to be selected. Each λ-stack composed of 20 *x*-*y* images at emission wavelengths separated by 10-nm (slit bandwidth) steps was collected within the spectral range of 464 to 663 nm for all specimens. The emission signals in each spectral band were acquired by a highly sensitive meshless PMT detector. The signals in a λ-stack were then linearly unmixed in the mTFP and mKO2 emission channels using the "dye separation" function of the LAS AF software. Data analysis of the unmixed images was carried out in our PFRET software; the algorithm used for sFRET microscopy in the software was described earlier.[10]

2.2.3 *Instrumentation for fluorescence lifetime imaging (FLIM)*

The fluorescence lifetime refers to the average time that the molecule stays in its excited state before emitting a photon, which is an intrinsic property of a fluorophore. There are different ways for measuring the fluorescence lifetime of a fluorophore[8]—we used the time-correlated single photon counting (TCSPC) method. The imaging system was described earlier in the literature.[31] Briefly, lifetime measurements in this study were made using a Nikon TE300 epifluorescence microscope equipped with a Plan Fluor 60×/1.20 NA water-immersion IR objective lens. This microscope was coupled to a Biorad Radiance 2100 confocal/multiphoton system and a 10-W Verdi pumped, tunable (700 to 1000 nm) mode-locked ultrafast (78 MHz) pulsed (150 femtosecond) laser (Mira 900, Coherent, Inc.). The Radiance 2100 system is controlled using LaserSharp2000 software and was configured to use the multiphoton laser to scan specimens. Emitted photons were collected using a bandpass emission filter by a fast PMT with a response time of approximately 150 picoseconds (PMC-100-0, Becker & Hickl GmbH, Berlin, Germany). The usage of the photon-counting module board (SPC-150, Becker & Hickl GmbH) with a minimum temporal resolution of approximately 40 picoseconds allowed pixel-by-pixel registration of the accumulated photons. A fluorescence decay histogram of photons at different emission times relative to the laser excitation was generated from the distribution of interpulse intervals at each pixel of the image.

2.2.4 *Image acquisition and analysis in lifetime measurements*

For FLIM-FRET, we measure only the change in lifetime for the donor molecule. Cells expressing mTFP alone were used to determine the unquenched donor lifetime, while cells expressing the mTFP-5aa-mKO2 construct were used to determine the quenched donor lifetime. The laser was tuned to 870 nm (the peak excitation of mTFP)[19] for multiphoton excitation, and the emission signal from mTFP was collected using a 480/40-nm emission filter. The fluorescence lifetime of mKO2 was determined by tuning the multiphoton laser to 740 nm and used a 600/75-nm emission filter to acquire images of the cells expressing mKO2 alone. In our experience, we found that a majority of red fluorophores are excitable at 740 to 760 nm. The laser power at the specimen plane was measured using a power meter (SSIM-VIS-IR, Coherent, Inc.) and was within the range of 0.7 to 1.5 mW. The data were typically acquired over 120 s; resulting in the accumulation of enough photon counts on the PMT for analysis by either single or double exponential fitting. The lifetime results were then analyzed using SPCImage software (version 2.9.2.2989, Becker & Hickl GmbH), which allows mutliexponential curve fitting on a pixel-by-pixel basis using a weighted least-squares numerical approach.

2.2.5 *Measuring the instrument response function (IRF) of the FLIM system*

For time-domain FLIM measurements, fluorescence lifetimes are frequently comparable to both the excitation pulse width and the instrument response function (IRF) of a FLIM system. Therefore, to obtain fluorescence decays free from the instrumental distortions that result from the finite rise time, the width and the decay of the excitation pulse, and the detector and timing apparatus[32] a deconvolution technique must be applied to extract the undistorted fluorescence decays that are convolved with the IRF. Direct measurement of the IRF is usually necessary for time-domain FLIM data analysis, and can be either estimated from fluorescence decay data or experimentally measured. The IRF should be representative of the experimental conditions and thus is ideally measured under the same conditions used for the biological experiments. Conventionally, nondairy coffee creamer can be used to record the IRF of a FLIM system for visible light excitation.[33]

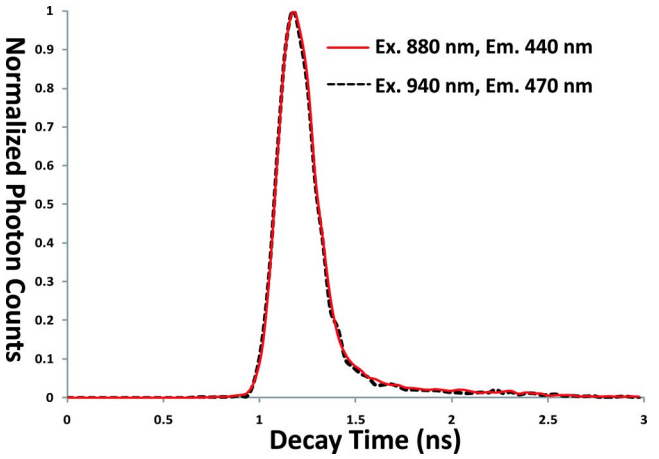

Fig. 1 Comparison of two measured instrument response functions (IRFs). Both IRFs were measured through collecting the second-harmonic generation (SHG) signals emitted from urea crystals. At the 880-nm excitation wavelength, the 440-nm SHG emission signals were collected using a 460/50-nm emission filter. Under the 940-nm excitation wavelength, the 470-nm SHG signals were collected using a 480/40-nm emission filter. The two IRFs (solid— the IRF measured at excitation 880 nm, emission 440 nm versus dashed—the IRF measured at excitation 940 nm, emission 470 nm) are almost overlaid with each other, confirming that the IRF did not change for the two different emission signals.

In this study, where infrared light excitation was used, we measured the IRF of the FLIM system through collecting the second-harmonic generation (SHG) signals emitted from urea crystals.[34] SHG is an ultrafast nonlinear process that delivers a signal at one-half the excitation wavelength. The IRFs were measured at both the 880-nm and the 940-nm excitation wavelengths. Although the 880-nm excitation wavelength was close to the one used for mTFP (870 nm), the SHG emission signals emitted at 440 nm had to be recorded using a 460/50-nm emission filter, which was different from the one used for mTFP (480/40 nm). Thus, the 940-nm excitation wavelength (although approaching the maximally allowed wavelength of the laser) was also used to measure the IRF, where the SHG signals emitted at 470 nm were collected using the 480/40-nm emission filter. The comparison between the two IRFs (Fig. 1) shows that they are almost identical. This fact confirmed that the IRF did not change from the 880-nm to the 940-nm excitation wavelengths and from the 440-nm to the 470-nm emission wavelengths.

To verify the utility of the measured IRFs, we used Cresyl Violet dissolved in ethanol as a standard. This sample yields a single exponential decay, and its fluorescence lifetime measured at room temperature is about 2.87 ns (Ref. 35). The excitation wavelength for the Cresyl Violet sample was the same as the one used for mKO2. This excitation wavelength (740 nm) was even farther away from the 880-nm excitation wavelength used in the IRF measurements than the mTFP excitation wavelength (870 nm). The peak emission wavelength of the Cresyl Violet sample is at 626 nm and was farther separated from the 470-nm emission wavelength in the IRF measurements than the mTFP (492 nm) or the mKO2 (565 nm) peak emission wavelength. The Cresyl Violet decays were collected using a 600/75-nm emission filter. Three

Table 1 The characteristics of mTFP and mKO2.

FP	Peak excitation	Peak emission	Quantum yield	Extinction coefficient[a]	Intrinsic brightness[b]
Teal	462	492	0.85	64	54
mKO2	551	565	0.62	63.8	53

[a]($\times 10^{-3}$) ($M^{-1}\,cm^{-1}$).
[b]Intrinsic brightness is the product of quantum yield and the extinction coefficient (see Ref. 20).

image (each has 128×128 pixels) data sets were acquired, and single exponential fitting of all the decay traces in these data sets using SPCImage software and the measured IRF yielded an average lifetime of 2.95 ns and a mean χ^2 of 1.05. In comparison, we also used the same routine to fit the data with the estimated IRF produced by SPCImage software and obtained an average lifetime of 3.19 ns and a mean χ^2 of 1.19. Although the excitation and emission wavelengths of the Cresyl Violet sample were much different than those in the IRF measurements, it still produced better fitting results. Therefore, the measured IRF was used for fitting the mTFP, mTFP-5aa-mKO2, and mKO2 data sets.

3 Results and Discussion

3.1 *Photophysical Properties of mTFP and mKO2*

The photophysical properties of a fluorophore, such as quantum yield and extinction coefficient (brightness), photostability, as well as the characteristics of the excitation and emission spectra all have important implications in FRET studies. The donor should have a high quantum yield, and ideally be of similar brightness to the acceptor. In this regard, mTFP has a higher quantum yield of 0.85 than mKO2 (0.62) and nearly identical brightness of mKO2 (Table 1). Both mTFP and mKO2 are very photostable, making them an attractive FRET pair in live-cell time-lapse imaging experiments. Furthermore, the spectral overlap between mTFP and mKO2 is greater than 50%, making them an excellent pair for detecting varying separation distances by measuring FRET efficiencies (Fig. 2). The dependence of FRET efficiency ($E\%$) on the distance (r) between the donor and the acceptor is described as

$$E\,\% = \frac{Ro^6}{Ro^6 + r^6} \quad , \tag{1}$$

where Ro is the Förster distance at which the efficiency of energy transfer is 50%. The Ro value for the mTFP-mKO2 FRET pair was calculated as 5.29 nm using the equation:

$$Ro = 0.211 \cdot [\kappa^2 \cdot n^{-4} \cdot QY_D \cdot J(\lambda)]^{1/6}, \tag{2}$$

where κ^2 ranging from 0 to 4 is the dipole orientation factor and here is assumed to be 2/3 (Ref. 36). n is the refractive index of the medium and is set to be 1.4. QY_D is the quantum yield of the donor (mTFP). $J(\lambda)$ expresses the degree of spectral overlap between the donor emission and the acceptor absorption (Fig. 2) and is calculated as follows:

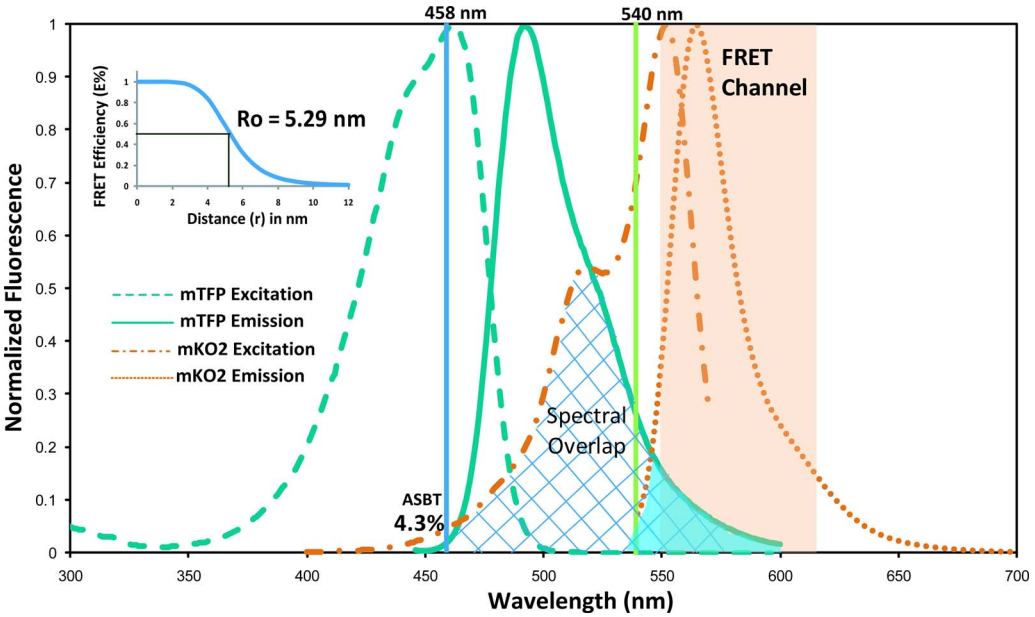

Fig. 2 Excitation and emission spectra of mTFP and mKO2. The spectra of mTFP and mKO2 are available from Allele Biotechnology and MBL International, respectively (see Sec. 2.1.1). The spectral overlap between the mTFP emission and the mKO2 excitation spectra (cross-hatched) is more than 50%; the 458-nm argon laser used for exciting the donor (mTFP) is almost at its peak excitation wavelength (462 nm); the 540-nm excitation wavelength was selected from the WLL to excite the acceptor (mKO2). Excitation of mKO2 at the 458-nm donor laser excitation determines the acceptor spectral bleedthrough (ASBT) and is low at 4.3%. The donor spectral bleedthrough (DSBT) is relative to the spectral overlap between the mTFP and the mKO2 emission spectra (shaded). The Förster distance (Ro=5.29 nm) for mTFP and mKO2 was calculated using Eqs.(2) and (3) (see Sec. 3.1).

$$J(\lambda) = \frac{\int_0^\infty f_D(\lambda)\epsilon_A(\lambda)\lambda^4 d\lambda}{\int_0^\infty f_D(\lambda)d\lambda} = \epsilon_A \frac{\int_0^\infty f_D(\lambda)f_A(\lambda)\lambda^4\, d\lambda}{\int_0^\infty f_D(\lambda)d\lambda}, \quad (3)$$

where f_D is the donor emission spectrum; $\varepsilon_A(\lambda)$ in units of $M^{-1}\cdot cm^{-1}$ is the extinction coefficient of the acceptor at λ in nanometers; ε_A is the extinction coefficient of the acceptor at its peak absorption wavelength; and f_A is the normalized acceptor absorption spectrum (peak absorbance is 1). The two integrals were calculated using a numerical integration program. We used the well-established enhanced cyan fluorescent protein (ECFP)-enhanced yellow fluorescent protein (EYFP) FRET pair to test the program. Given the normalized ECFP emission and EYFP absorption spectra, the ECFP quantum yield (0.4), the EYFP extinction coefficient (84,000), and the typical κ^2 and n values to the program, we obtained the Förster distance of this pair as 4.91 nm, which well matches the value (4.92 ± 0.1 nm) reported in the literature.[37]

The considerable spectral overlap, which is a requirement for efficient FRET, also gives rise to the background DSBT and ASBT that contaminate the FRET signal. In this respect, the mKO2 emission spectral overlap with the mTFP emission spectrum (Fig. 2) is reduced compared to the overlap of the yellow FPs with mTFP. Further, because mKO2 is more red-shifted, the excitation percentage of mKO2 (4.3%) at the 458-nm wavelength, used for mTFP is less than half that for Venus or EYFP 9.6%, their spectra are not shown; (Fig. 2). For spectral FRET measurements, the DSBT is removed through linear unmixing (discussed in the following), so the reduced ASBT makes mKO2 a good acceptor for sFRET microscopy.

To date, many of the currently available orange or red FPs have not proven to be useful acceptors for spectral FRET (sensitized emission) measurements (mCherry and mOrange, for example). Of course, EYFP suffers from problems with pH and halide sensitivity, and has been replaced by Citrine or Venus. The primary advantages of mKO2 over Venus are improved photostability, reduced spectral bleedthrough, and red-shifted acceptor emission. Citrine does have improved photostability, but it has the same spectral characteristics as Venus.

3.2 *E% of mTFP-5aa-mKO2 in sFRET Microscopy*

Spectral FRET (sFRET) microscopy utilizes linear unmixing, which provides one of the most accurate methods for removing the contribution of DSBT from the FRET channel.[10,38,39] Here, signals were acquired at different spectral bands in a λ-stack [Figs. 3(A)–3(C); see Sec. 2.2.2], and were then decomposed and reassigned to the donor (mTFP) and the acceptor (mKO2) emission channels through linear unmixing, a mathematical algorithm that defines the spectral signature for each pixel of the scanned confocal image and allows the digital separation of the component signals. The reference spectra used for unmixing and removal of the DSBT signals were obtained from cells expressing either mKO2 alone [Fig. 3(C); solid] or mTFP alone [Fig. 3(D)]. However, the ASBT and the FRET signal are combined in the acceptor emission spectrum. To determine the contribution of ASBT to the FRET signal, we acquired the λ-stacks from the double-labeled (mTFP-5aa-mKO2) cells excited by the acceptor excitation [Fig. 3(B)] and the λ-stacks of the mKO2-alone cells using both the donor and the acceptor excitation wavelengths [Fig. 3(C)]. Criti-

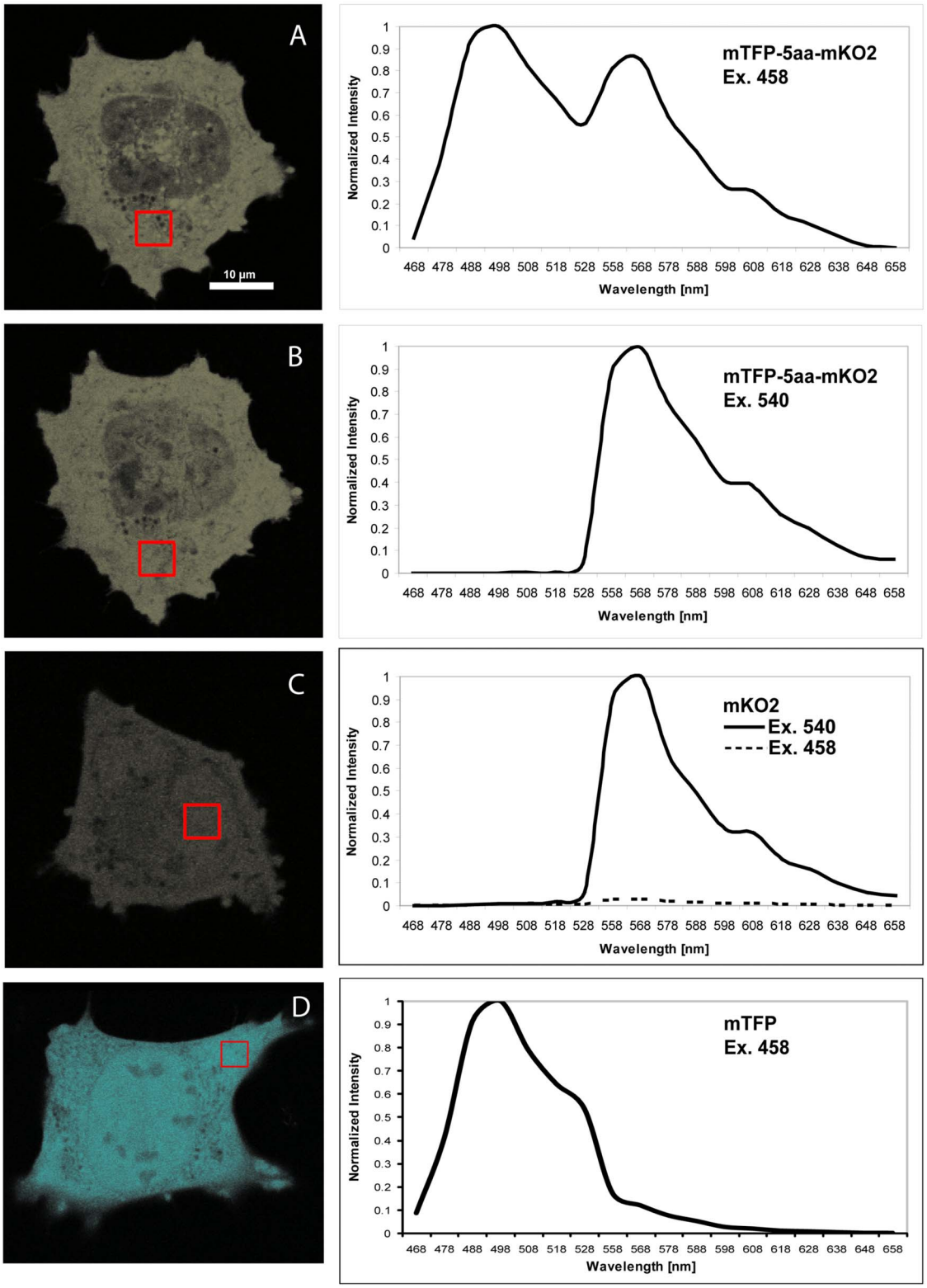

Fig. 3 Data acquisition in sensitized spectral FRET (sFRET)microscopy. λ-stacks in sFRET microscopy for evaluating *E*% of mTFP-5aa-mKO2 were acquired with both the donor (458 nm) and the acceptor (540 nm) excitation wavelengths. (a) The emission spectrum was plotted from the λ-stacks acquired from an mTFP-5aa-mKO2 cell excited by the 458-nm argon laser. The emission signals at 568 nm clearly indicate sensitized FRET signals, although the spectrum still contains both donor and acceptor spectral bleedthroughs. (b) The same cell was also excited by the 540-nm wavelength selected from the WLL, and the emission spectrum was plotted. (c) As discussed in Sec. 3.2, to remove the acceptor spectral bleedthrough (ASBT) from FRET signals, the acceptor-alone expressed cells were excited by both the donor and the acceptor excitation wavelengths, and the emission spectra of one selected cell were plotted. The two emission spectra were normalized by the same factor. The comparison between the two emission spectra produced by the acceptor (solid line) and the donor (dashed line) excitations indicates that the ASBT was trivial. Reference spectra of (c) mKO2 (solid) and (d) mTFP for linear unmixing were extracted from the λ-stacks collected from singly expressed cells.

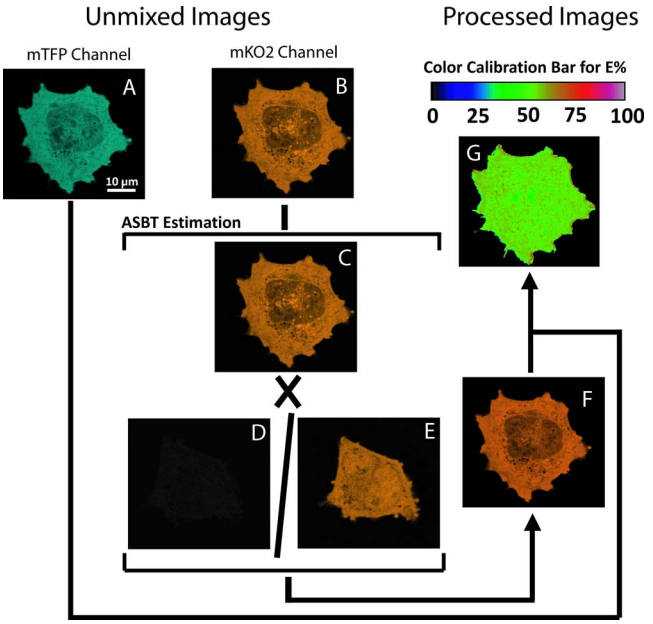

Fig. 4 Data processing in sensitized spectral FRET (sFRET) microscopy. All mTFP-5aa-mKO2 and mKO2-alone λ-stacks acquired by spectral imaging were linearly unmixed, and signals in each λ-stack were decomposed into the mTFP and the mKO2 emission channels. The amount of the quenched donor [*qDonor*; (a)] signals in the mTFP emission channel was unmixed from the λ-stack acquired by exciting the mTFP-5aa-mKO2 cell with the donor excitation. The image at the mKO2 emission channel unmixed from the same λ-stack included both the FRET and the acceptor spectral bleedthrough (ASBT) signals, called the uncorrected spectral FRET [usFRET; (b)] image. ASBT was determined from the image at the mKO2 emission channel unmixed from the λ-stack acquired from the same mTFP-5aa-mKO2 cell excited by the acceptor excitation (c), and also the images at the mKO2 emission channel unmixed from the λ-stacks obtained through exciting the mKO2-alone cell with both the donor (d) and the acceptor (e) excitation wavelengths. The unmixed images were then processed using the established PFRET software (see Sec. 2.2.2) to obtain the processed spectral FRET [psFRET; (f)] image. Based on Eq. (3) and given the *qDonor* and psFRET values at each pixel, the apparent FRET efficiency [*E*%; (g)] image was calculated.

cally, we observed that the DPSS 561-nm laser was not suitable for the sensitized FRET microscopy measurements using mKO2 as an acceptor because it is very close to the peak emission for this fluorophore (565 nm; Table 1). Since at least 5 nm must separate the acceptor excitation wavelength and the beginning of the spectral FRET measurement, using the 561-nm laser for acceptor excitation resulted in a significant loss of the sensitized acceptor emission from mKO2. In this regard, the WLL provided a distinct advantage, since it was possible to fine-tune the excitation to 540 nm and thus a wider emission detection range for an optimal FRET signal. Meanwhile, the excitation of mKO2 at the 540-nm wavelength was sufficient for the purpose of determining ASBT. It should be noted that the autofluorescence from the used live cells excited along the visible spectrum under normal imaging conditions was not observed.

We have shown in Fig. 4 a complete sequence of images required for sFRET data analysis using PFRET software (see Sec. 2.2.2). Figures 4(A) and 4(B) show the quenched donor (*qDonor*) and the uncorrected sFRET (usFRET) images, respectively. Both of them were obtained from unmixing the λ-stack of mTFP-5aa-mKO2 excited by the donor excitation: [Fig. 3(A)]. Figure 4(C) is the acceptor fluorescence image obtained from unmixing the λ-stack of mTFP-5aa-mKO2 excited by the acceptor excitation [Fig. 3(B)]. These three unmixed images were then processed in PFRET software using the unmixed single-label reference images of the acceptor acquired with the donor excitation [Fig. 4(D)] and the acceptor excitation [Fig. 4(E)]. This then produces the processed spectral FRET (psFRET) image [Fig. 4(F)], where the signal at each pixel is obtained by subtracting the ASBT that is determined from the corresponding pixel in the usFRET image. The apparent FRET efficiency ($E\%$) is displayed as an image [Fig. 4(G)], where the value at each pixel is calculated based on Eq. (4) using the corresponding pixel values in the psFRET and *qDonor* images:

$$E\% = \frac{psFRET}{(s_A/s_D)\cdot(QY_A/QY_D)\cdot qDonor + psFRET}, \quad (4)$$

where the term $(S_A/S_D)\cdot(QY_A/QY_D)$ is a coefficient (0.9355), which was used for linking the intensity of the *qDonor* from the donor emission channel with the corresponding intensity appearing in the acceptor emission channel. Detailed explanation about this coefficient can be found in Ref. 8. Briefly, S_A and S_D are the PMT spectral sensitivities at the peak emission wavelength of mTFP and mKO2, respectively. QY_A and QY_D are the quantum yields of mTFP and mKO2, respectively.

$E\%$s evaluated from different regions of one cell [Fig. 4(G)] or different cells (Table 2) have a very small variation (standard deviation=1.33 for six cells with average $E\%$ =54.76), which was expected for the mTFP-5aa-mKO2 fusion protein since the distance variations between mTFP and mKO2 are minimized by using the 5aa linker. Given the average $E\%$ of mTFP-5aa-mKO2 (54.76) and the Förster distance of mTFP-mKO2 (5.29 nm) to Eq. (1), the average distance between mTFP and mKO2 was estimated to be 5.12 nm. In addition, the SBT correction (SBT%) for this fluorophore pair, which is defined as ASBT/usFRET or 1-psFRET/usFRET, was small (Table 2), which is also consistent with our expectations based on the mTFP and mKO2 excitation and emission spectra (see Sec. 3.1 and Fig. 2). Apart from generating the psFRET and $E\%$ images [Figs. 4(F) and 4(G)], the PFRET software produces a full data set with the option of creating a set of regions of interest (ROIs) and statistical evaluation.

While the sFRET results for mKO2 as an acceptor using the WLL system are very promising, we suggest that a fixed HeNe 543-nm laser system might be equally suitable. We compared results using the 540-nm and 543-nm wavelengths on the WLL on the same specimen and found no noticeable difference.

3.3 *Confirmation of E% of mTFP-5aa-mKO2 Using FLIM-FRET Microscopy*

Since FRET is a dynamic process that nonradiatively depopulates the excited-state donor fluorophores, it can also be determined by measuring the reduction in the donor fluorescence lifetime that results from quenching. In fluorescence

Table 2 Spectral FRET results of mTFP-5aa-mKO2.

Data set	Number of pixels[a]	usFRET[b]	psFRET[b]	*SBT*%[b,c]	*qDonor*[b]	*E*%[b]
1	18290	1525	1475	3.42	1871	55.21
2	15987	1051	1004	4.63	1227	56.25
3	45284	1895	1844	2.79	2543	53.27
4	25083	1761	1711	3.01	2124	55.85
5	26571	1748	1698	3.01	2354	53.05
6	59326	2119	2069	2.53	2655	54.96
Mean	**31756**	**1683**	**1633**	**3.23**	**2129**	**54.76 ±1.33**[d]

[a]To remove background noise, a threshold was applied to the uncorrected FRET images for pixel analysis.
[b]For each given variable, the mean value over all analyzed pixels was calculated.
[c]*SBT*% was determined by 1 – psFRET/usFRET at a pixel-based level.
[d]±standard deviation, calculated from the data (six cells) in the *E*% column.

lifetime imaging (FLIM) microscopy, the energy transfer efficiency ($E\%$) between the donor and the acceptor can be calculated from the donor fluorescence lifetimes determined in the absence (τ_D—unquenched lifetime) and in the presence (τ_{DA}—quenched lifetime) of an acceptor using the equation:

$$E\% = 1 - \tau_{DA}/\tau_D. \quad (5)$$

To determine the unquenched lifetime (τ_D) of mTFP, we acquired data sets from the cells that were labeled only with mTFP (see Sec. 2.2.4). These data sets were then analyzed using SPCImage software based on a single-exponential decay model. Given the input of the measured instrument response function (IRF), the fitting routine yielded an average unquenched mTFP lifetime of 2.684 ns (see Secs. 2.2.4 and 2.2.5). Better approximation of the data was not observed from the double-exponential fitting of these data sets, which did not produce and a significant difference between the faster (2.6 ns) and slower (2.8 ns) lifetime components.

Using SPCImage software and the same measured IRF, we performed both single and double exponential fittings on the data sets acquired from the mTFP-5aa-mKO2 expressed cells. The monoexponential model was rejected because the biexponential model yielded a much better approximation of the data in terms of χ^2, residuals, and visually comparing the fitting curves with the raw data. The obtained average quenched lifetime (τ_{DA}) of mTFP was 1.111 ns. There are many reasons to explain why a monoexponential decay cannot be observed even though mTFP and mKO2 were tethered by a 5aa linker. For example, FRET requires not only a close distance between donor and acceptor, but also a favorable orientation between the dipoles of the donor emission and the acceptor absorption, which may not be satisfied for all mTFP-5aa-mKO2 constructs. Another cause might be that the linking peptide chain is flexible, where donor and acceptor fluorophores are not separated by a single distance rather than a distance distribution. Moreover, occasional incomplete synthesis or protein misfolding cannot be ruled out.

We also confirmed that the mTFP-5aa-mKO2 decay did not contain any measurable autofluorescence or back-bleedthrough of mKO2 excited at the 870-nm wavelength. Verifications were made through imaging the mKO2-alone cells under the same imaging conditions used for collecting the mTFP-5aa-mKO2 decay data, where no signal other than background noise was observed.

Figure 5(A) demonstrates the decay rate differences between the mTFP without mKO2 and the mTFP in the presence of mKO2. Figure 5(F) provides representative examples of the processed data of mTFP and mTFP-5aa-mKO2. Table 3 lists the different data sets of the donor lifetime in the presence of acceptor. The significant fitting was performed as indicated by the χ^2 value. The quenched lifetime (τ_{DA}) of mTFP was determined, and by applying the unquenched lifetime of mTFP (2.684 ns) to Eq. (5), we calculated $E\%$, resulting in an average FRET efficiency of approximately 58.63% (Table 3), which is close to that (54.76%) obtained from spectral FRET microscopy imaging (Table 2). The linked fluorophores used here provided a FRET standard[26] to test the utility of this FRET pair, allowing us to confirm accurately the sFRET results by FLIM-FRET measurements. With this standard, we would expect a very low level of non-FRET donors and as a consequence a narrow range of lifetimes as well as $E\%$s.

3.4 *Lifetime of mKO2 Expressed in Live Mouse Pituitary GHFT1 Cells*

We also evaluated the lifetime of mKO2 through acquiring data sets from the cells that were labeled only with mKO2 (see Sec. 2.2.4). The average lifetime was obtained as 3.14 ns through single exponential fittings of the mKO2-alone data sets ($n=6$) in the SPCImage software given the same measured IRF as used in the FLIM-FRET data analyses earlier. A representative decay fitting curve of mKO2 is shown in Fig. 5(A).

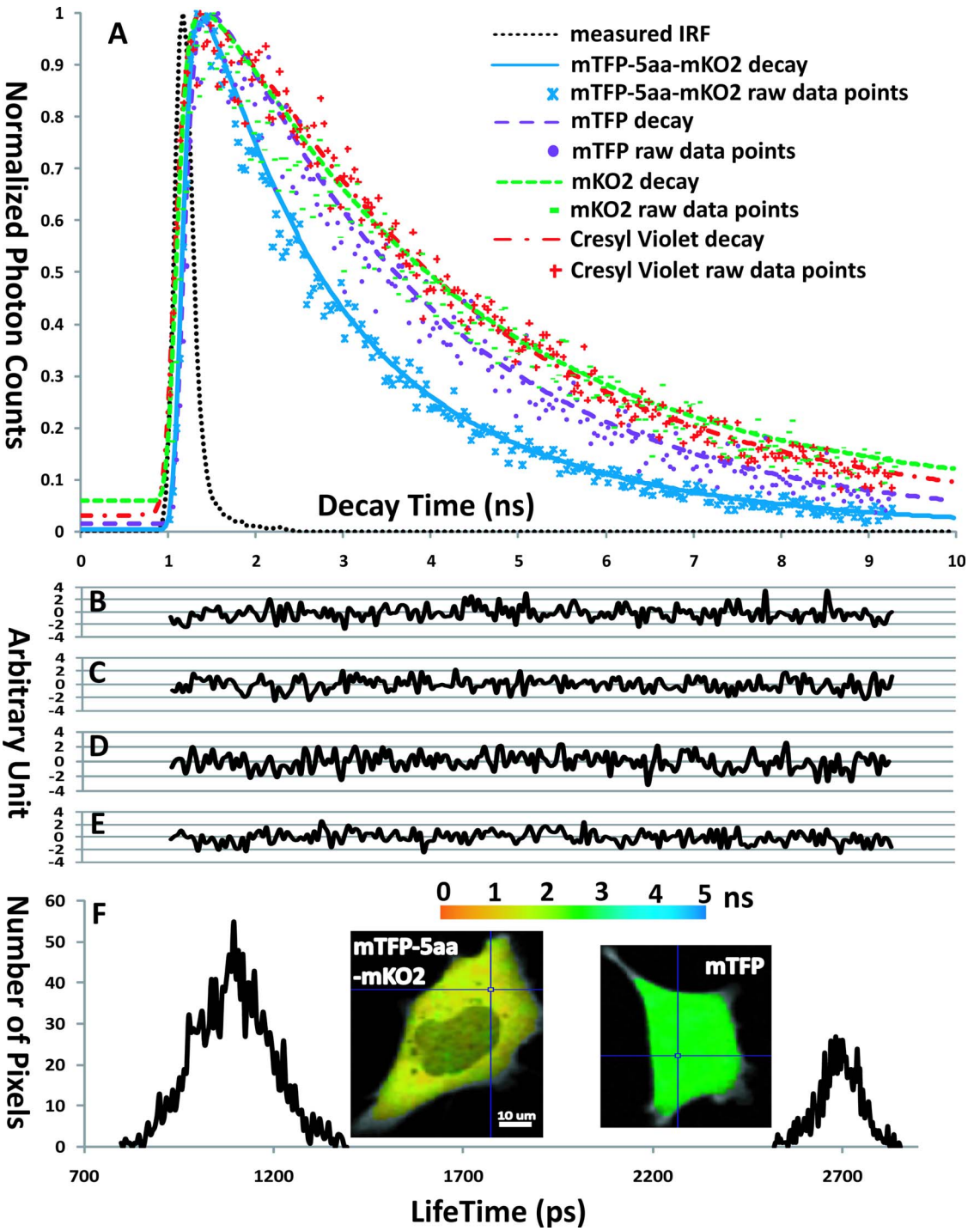

Fig. 5 Data analysis in FLIM-FRET microscopy. Change in donor (mTFP) lifetime in the absence and the presence of the acceptor (mKO2) was measured from cells expressing mTFP alone or mTFP-5aa-mKO2, respectively. The fluorescent lifetime decay kinetics for mTFP (donor) alone and in the presence of mKO2 (acceptor) were determined by fitting the data into a single or double exponential decay, respectively. These lifetimes were estimated using our measured instrument response function (IRF) (see Sec. 2.2.5). The measured IRF (300 picoseconds at FWHM) of the FLIM system (dotted line) is shown in (a), where the fitting curve and the raw data points of Cresyl Violet in ethanol (dotted-dashed line and +) used for verifying the utility of the measured IRF (see Sec. 2.2.5) is also shown. The comparison between the decay curves and the raw data points (a) clearly shows mTFP-5aa-mKO2 (solid line and ×) decayed faster than mTFP (coarse dashed line and °), since mTFP was quenched by mKO2 due to FRET (see Secs. 2.2.4 and 3.3). The representative single-exponential decay curve together with the corresponding raw data points of mKO2 (fine dashed line and –) expressed in mKO2 single-label cells is also shown in (a) (see Secs. 2.2.4 and 3.4). The corresponding residuals of the mTFP-5aa-mKO2, mTFP, mKO2, and Cresyl Violet fitting curves are shown in (b), (c), (d), and (e) with the same nanosecond (ns) scale used in (a), respectively. The lifetime distributions for quenched (left: mTFP-5aa-mKO2) and unquenched (right: mTFP) mTFP are shown in (f) with a picosecond (ps) time scale. A wider distribution of the quenched mTFP lifetime was observed, compared to the unquenched mTFP, since the distance variations existed between the mTFP and mKO2 folded proteins in cells even though they were tethered by a 5 amino acid linker (see Sec. 3.3).

Table 3 FLIM-FRET results of mTFP-5aa-mKO2.

Data set[a]	χ^2	τ_{DA} (ns)[b]	E%[c]
1	1.10	1.121	58.23
2	1.14	1.157	56.89
3	1.11	1.081	59.72
4	1.10	1.092	59.31
5	1.13	1.110	58.64
6	1.14	1.102	58.94
Mean	**1.12**	**1.111**	**58.63±0.99**[d]

[a]While identical specimens were used for lifetime measurements and sensitized sFRET microscopy, the actual regions of interest (cells) are different, since data was collected on two different systems.
[b]τ_{DA} (in nanoseconds) is the lifetime of the quenched mTFP measured from cells labeled with the mTFP-5aa-mKO2 construct.
[c]E% is determined by Eq. (5), where τ_D is the unquenched mTFP lifetime measured from the cells labeled only with mTFP, equal to 2.684 ns (see Sec. 3.3).
[d]±standard deviation, calculated from the data (six cells) in the E% column.

4 Conclusions

Genetically encoded fluorescent proteins (FPs) used in combination with sensitized FRET microscopy provide important tools for detecting protein interactions in their natural environment within living cells. The orange FPs are the most attractive acceptor candidates, bridging the gap between green and red FPs. In this study, we demonstrated that a newly developed orange FP—mKO2—is a suitable acceptor for mTFP, provided optimal excitation wavelengths and emission ranges are available to collect a robust FRET signal. mTFP as a FRET donor has many advantages over CFP and Cerulean.[19] The FRET efficiency of the mTFP-5aa-mKO2 construct measured in live cells was about 54.8% in sFRET microscopy and 58.6% in FLIM-FRET microscopy, showing a good match (see Secs. 3.2 and 3.3). The photophysical properties of mTFP and mKO2 suggest that they are a good FRET pair, especially when they are used in sFRET microscopy, because of the low absorption of mKO2 at the donor excitation wavelength of mTFP (see Sec. 3.1). In our spectral FRET experiments, the excitation for mKO2 was chosen from a white-light laser (WLL) allowing a tunable excitation wavelength from 470 to 670 nm in 1-nm increments. We believe that the WLL will extend the number of usable FRET pairs in general and in particular those that are orange and red FPs. However, the usage of mKO2 as an acceptor in sensitized FRET microscopy assays is not limited to a WLL, since a HeNe 543-nm laser should be equally suitable for this FRET pair (see Sec. 3.2).

Acknowledgments

The authors thank Horst Wallrabe for his suggestions and critical reading of this manuscript and Sydney Provence for preparing the graphs in this manuscript. We greatly appreciate the help provided by Drs. Scott Young and Haridas Pudavar, Leica Microsystems, Inc., Germany. This work was supported by an award from the National Center for Research Resources, National Institutes of Health (RR025616).

References

1. R. Y. Tsien, "The green fluorescent protein," *Annu. Rev. Biochem.* **67**, 509–544 (1998).
2. B. N. Giepmans, S. R. Adams, M. H. Ellisman, and R. Y. Tsien, "The fluorescent toolbox for assessing protein location and function," *Science* **312**, 217–224 (2006).
3. R. N. Day and F. Schaufele, "Fluorescent protein tools for studying protein dynamics in living cells: a review," *J. Biomed. Opt.* **13**, 031202 (2008).
4. D. W. Piston and G.-J. Kremers, "Fluorescent protein FRET: the good, the bad and the ugly," *Trends Biochem. Sci.* **32**, 407–414 (2007).
5. R. B. Sekar and A. Periasamy, "Fluorescence resonance energy transfer (FRET) microscopy imaging of live cell protein localizations," *J. Cell Biol.* **160**, 629–633 (2003).
6. T. Förster, "Delocalized excitation and excitation transfer," in *Modern Quantum Chemistry*, O. Sinanoglu, Ed., Vol. **3**, pp. 93–137, Academic Press, Inc., New York (1965).
7. R. M. Clegg, "Fluorescence resonance energy transfer," *In Fluorescence Imaging Spectroscopy and Microscopy*, X. F. Wang and B. Herman, Eds., Vol. **137**, pp. 179–251, John Wiley & Sons, Inc., New York (1996).
8. Y. Chen, M. Elangovan, and A. Periasamy, "FRET data analysis—the algorithm," Chapter 7 in *Molecular Imaging: FRET Microscopy and Spectroscopy*, A. Periasamy and R. N. Day, Eds., pp. 126–145, Oxford University Press, New York (2005).
9. Y. Chen and A. Periasamy, "Intensity range based quantitative FRET data analysis to localize protein molecules in live cell nuclei," *J. Fluoresc.* **16**, 95–104 (2006).
10. Y. Chen, J. P. Mauldin, R. N. Day, and A. Periasamy, "Characterization of spectral FRET imaging microscopy for monitoring nuclear protein interactions," *J. Microsc.* **228**, 139–152 (2007).
11. H. Wallrabe and A. Periasamy, "Imaging protein molecules using FRET and FLIM microscopy," *Curr. Opin. Biotechnol.* **16**, 19–27 (2005).
12. J. Zhang, R. E. Campbell, A. Y. Ting, and R. Y. Tsien, "Creating new fluorescent probes for cell biology," *Nat. Rev. Mol. Cell Biol.* **3**, 906–918 (2002).
13. G. Patterson, R. N. Day, and D. Piston, "Fluorescent protein spectra," *J. Cell. Sci.* **114**, 837–838 (2001).
14. R. Heim and R. Y. Tsien, "Engineering green fluorescent protein for improved brightness, longer wavelengths and fluorescence resonance energy transfer," *Curr. Biol.* **6**, 178–182 (1996).
15. M. Ormö, A. B. Cubitt, K. Kallio, L. A. Gross, R. Y. Tsien, and S. J. Remington, "Crystal structure of the *Aequorea victoria* green fluorescent protein," *Science* **273**, 1392–1395 (1996).
16. T. Nagai, K. Ibata, E. S. Park, M. Kubota, K. Mikoshiba, and A. Miyawaki, "A variant of yellow fluorescent protein with fast and efficient maturation for cell-biological applications," *Nat. Biotechnol.* **20**, 87–90 (2002).
17. M. A. Rizzo, G. H. Springer, B. Granada, and D. W. Piston, "An improved cyan fluorescent protein variant useful for FRET," *Nat. Biotechnol.* **22**, 445–449 (2004).
18. H. W. Ai, N. J. Henderson, S. J. Remington, and R. E. Campbell, "Directed evolution of a monomeric, bright and photostable version of Clavularia cyan fluorescent protein: structural characterization and applications in fluorescence imaging," *Biochem. J.* **400**, 531–540 (2006).
19. R. N. Day, C. F. Booker, and A. Periasamy, "Characterization of an improved donor fluorescent protein for Förster resonance energy transfer microscopy," *J. Biomed. Opt.* **13**, 031203 (2008).
20. N. C. Shaner, R. E. Campbell, P. A. Steinbach, B. N. Giepmans, A. E. Palmer, and R. Y. Tsien, "Improved monomeric red, orange and yellow fluorescent proteins derived from *Discosoma sp.* red fluorescent protein," *Nat. Biotechnol.* **22**, 1567–1572 (2004).
21. N. C. Shaner, P. A. Steinbach, and R. Y. Tsien, "A guide to choosing fluorescent proteins," *Nat. Methods* **2**, 905–909 (2005).
22. N. C. Shaner, G. H. Patterson, and M. W. Davidson, "Advances in fluorescent protein technology," *J. Cell. Sci.* **120**, 4247–4260 (2007).
23. N. C. Shaner, M. Z. Lin, M. R. McKeown, P. A. Steinbach, K. L. Hazelwood, M. W. Davidson, and R. Y. Tsien, "Improving the photostability of bright monomeric orange and red fluorescent proteins," *Nat. Methods* **5**, 545–551 (2008).
24. S. Karasawa, T. Araki, T. Nagai, H. Mizuno, and A. Miyawaki, "Cyan-emitting and orange-emitting fluorescent proteins as a donor/

acceptor pair for fluorescence resonance energy transfer," *Biochem. J.* **381**, 307–312 (2004).
25. A. Sakaue-Sawano, H. Kurokawa, T. Morimura, A. Hanyu, H. Hama, H. Osawa, S. Kashiwaqi, K. Fukami, T. Miyata, H. Miyoshi, T. Imamura, M. Ogawa, H. Masai, and A. Miyawaki, "Visualizing spatiotemporal dynamics of multicellular cell-cycle progression," *Cell* **132**, 487–498 (2008).
26. S. V. Koushik, H. Chen, C. Thaler, H. L. Puhl III, and S. S. Vogel, "Cerulean, Venus, and VenusY67C FRET reference standards," *Biophys. J.* **91**, L99–L101 (2006).
27. D. Lew, H. Brady, K. Klausing, K. Yaginuma, L. E. Theill, C. Stauber, M. Karin, and P. L. Mellon, "GHF-1-promoter-targeted immortalization of a somatotropic progenitor cell results in dwarfism in transgenic mice," *Genes Dev.* **7**, 683–693 (1992).
28. R. N. Day, A. Periasamy, and F. Schaufele, "Fluorescence resonance energy transfer microscopy of localized protein interactions in the living cell nucleus," *Methods* **25**, 4–18 (2001).
29. J. F. Enwright, M. A. Kawecki-Crook, T. C. Voss, F. Schaufele, and R. N. Day, "A PIT-1 homeodomain mutant blocks the intranuclear recruitment of the CCAAT/enhancer binding protein alpha required for prolactin gene transcription," *Mol. Endocrinol.* **17**, 209–222 (2003).
30. K. Jalink, A. Diaspro, V. Caorsi, and P. Bianchini, "Solving the challenge of fluorescence Leica TCS SP5 X: the first completely tunable confocal system," Confocal Application Letter 29 (August 2008), www.leica-microsystems.com/products/confocal-microscopes/details/product/leica-tcs-sp5-x/.
31. Y. Chen and A. Periasamy, "Characterization of two-photon excitation fluorescence lifetime imaging microscopy for protein localization," *Microsc. Res. Tech.* **63**, 72–80 (2004).
32. I. Gryczynski, R. Luchowski, S. Bharill, J. Borejdo, and Z. Gryczynski, "Non-linear curve fitting methods for time-resolved data analysis," in *FLIM Microscopy in Biology and Medicine*, A. Periasamy and R. M. Clegg, Eds., pp. 341–370, CRC Press, New York (2009).
33. A. Periasamy, P. Wodnicki, X. F. Wang, S. Kwon, G. W. Gordon, and B. Herman, "Time-resolved fluorescence lifetime imaging microscopy using a picosecond pulsed tunable dye laser system," *Rev. Sci. Instrum.* **67**, 3722–3731 (1996).
34. W. Becker, "Recording the instrument response function of a multiphoton FLIM system," Application Notes, www.becker-hickl.com (2007).
35. D. I. Kreller and P. V. Kamat, "Photochemistry of sensitizing dyes. spectroscopic and redox properties of Cresyl Violet," *J. Phys. Chem.* **95**, 4406–4410 (1991).
36. J. R. Lakowicz, *Principles of Fluorescence Spectroscopy*, 3rd ed., Plenum, New York (2007).
37. G. H. Patterson, D. W. Piston, and B. G. Barisas, "Förster distances between green fluorescent protein pairs," *Anal. Biochem.* **284**, 438–440 (2000).
38. C. Thaler, S. V. Koushik, P. S. Blank, and S. S. Vogel, "Quantitative multiphoton spectral imaging and its use for measuring resonance energy transfer," *Biophys. J.* **89**, 2736–2749 (2005).
39. T. Zimmermann, J. Rietdorf, A. Girod, V. Georget, and R. Pepperkok, "Spectral imaging and linear un-mixing enables improved FRET efficiency with a novel GFP2-YFP FRET pair," *FEBS Lett.* **531**, 245–249 (2002).